Sonochemical degradation of bisphenol A using persulfate activated by hematite nanoparticles

Mahboobeh Dehvari, Farshid Ghanbari and Mehdi Ahmadi

ABSTRACT

In this study, hematite nanoparticles (HNPs) were used as the persulfate (PS) activator for the sonocatalytic degradation of bisphenol A (BPA). The physicochemical properties of the synthesized HNPs were investigated using X-ray diffraction (XRD), field emission scanning electron microscopy (FESEM), Fourier transform infrared spectroscopy (FTIR) and transmission electron microscopy (TEM). The effect of different operational parameters (pH, nanoparticle dosage, persulfate concentration, and ultrasonic power) on catalytic activity were evaluated. The BPA degradation rate was improved when ultrasonic (US) irradiation was used simultaneously with HNPs for activating PS. According to the results, 98.94% of BPA (10 mg/L) was degraded within 15 min of reaction time at 4 mM persulfate and 0.01 g/L HNPs under ultrasonic irradiation of 250 W. The degree of mineralization of BPA was measured using chemical oxygen demand (COD), and 36.98% was achieved under optimum conditions. Quenching tests were done using different scavenger compounds; these showed that both hydroxyl and sulfate radicals were reactive species in BPA degradation. According to the results of reusability tests, the degradation efficiency decreased to 86.34%, indicating that HNPs can be recycled several times. All of the anions tested, but mainly hydrogen phosphate, had an inhibitory effect on BPA degradation. The results showed that the US/HNPs/PS process is effective for the degradation of the organic pollutants.

Key words | advanced oxidation processes, bisphenol A, hematite, persulfate, ultrasonic irradiation

HIGHLIGHTS

- HNPs can effectively activate PS for the generation of $OH^{\bullet}$ and $SO_4^{\bullet-}$ radicals, which are strong oxidants for the degradation of BPA.
- The degradation rate was significantly improved when US irradiation was used simultaneously with HNPs.
- 98.94% of BPA was degraded at 4 mM PS and 0.01 g/L HNPs under US irradiation of 250 W for 15 min.
- Both hydroxyl and sulfate radicals were reactive species in BPA degradation.

Mahboobeh Dehvari
Student Research Committee,
Department of Environmental Health Engineering,
Ahvaz Jundishapur University of Medical Sciences,
Ahvaz,
Iran

Farshid Ghanbari
Department of Environmental Health Engineering,
Abadan Faculty of Medical Sciences,
Abadan,
Iran

Mehdi Ahmadi (corresponding author)
Environmental Technologies Research Center,
Department of Environmental Health Engineering,
Ahvaz Jundishapur University of Medical Sciences,
Ahvaz,
Iran
E-mail: *ahmadi241@gmail.com*

doi: 10.2166/wst.2020.592

GRAPHICAL ABSTRACT

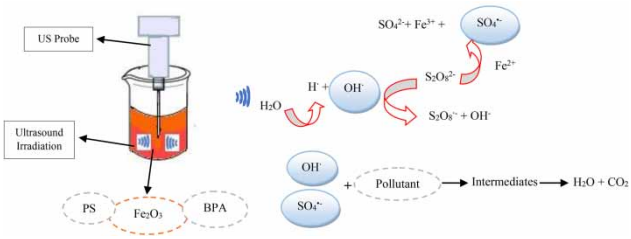

INTRODUCTION

Endocrine disrupting compounds (EDCs) contain a variety of toxic organic compounds (such as alkylphenol azoxylate, polychlorinated bisphenyls, insecticides, steroid sex hormones, polybromin compounds, phatalites, and bisphenol A), which are emerging contaminants in water resources (Staples *et al.* 1998; Vandenberg *et al.* 2009).

Bisphenol A (BPA; 4,4′-(propane-2,2-diyl)diphenol) is widely used as a monomer in the plastics industry to produce materials such as epoxy resins and polycarbonates; it is also used in various consumer products such as food packaging, PVC, and baby bottles. This pollutant is introduced into the environment by point and non-point sources (Staples *et al.* 1998; Vandenberg *et al.* 2009; Rochester 2013). Point sources include sewage sludge, landfill, raw sewage, and runoff. Non-point sources are polycarbonate plastics, residual epoxy resins, and synthetic polymers. BPA can penetrate underground water through industrial and agricultural wells (Staples *et al.* 1998; Huang *et al.* 2012). BPA levels reported in runoff and drinking water were 12 μg/L and 0.1 μg/L, respectively, and in some sources the detected concentrations were higher than 100 mg/L (Staples *et al.* 1998; Escalona *et al.* 2014). Very low levels of BPA lead to cardiovascular diseases, propagation of human prostate cancer cells, and type 2 diabetes (Mohapatra *et al.* 2010).

Different biological and chemical methods have been used to remove BPA from water and wastewater. Advanced oxidation processes (AOPs) are known to be the most effective method for degrading organic pollutants due to the production of reactive species such as hydroxyl radicals (˙OH) that have high oxidation potential ($E_0 = 2.8$ V). These processes include ozonation, Fenton reaction, photocatalysis, electrooxidation and sonochemical processes (Jiang *et al.* 2013; Escalona *et al.* 2014; Huang *et al.* 2021).

Nowadays, researchers have focused on sulfate-radical-based AOPs for the degradation of refractory organic pollutants (Mokhtari *et al.* 2016; Huang *et al.* 2021). The sulfate radical ($SO_4^{\bullet-}$), with a redox potential of 2.5–3.1 V, is one of the most commonly used oxidants and is produced by the activation of peroxymonosulfate (PMS, HSO_5^-) or persulfate (PS, $S_2O_8^{2-}$). The persulfate or peroxydisulfate ion attracts more attention than PMS, because it is cheaper, more stable and more suitable for water/wastewater decontamination (Lu *et al.* 2020). Activating agents such as transition metals, heat, ultraviolet (UV), and ultrasound (US), are applied to activate PS to produce sulfate radicals (Equation (1)) (Ji *et al.* 2011; Guan *et al.* 2013; Hu & Long 2016).

$$S_2O_8^{2-} + \text{activator} \rightarrow SO_4^{\bullet-} + (SO_4^{2-} \text{or } SO_4^{\bullet-}) \quad (1)$$

Among these agents, the transition metals are the most widely used. Iron is the most commonly used metal, as it is more cost-effective than other metals and relatively non-toxic. It can activate persulfate ($S_2O_8^{2-}$) to a sulfate radical, as shown in Equation (2) (Kusic *et al.* 2011; Liu *et al.* 2015; Li *et al.* 2016; Oh *et al.* 2016).

$$S_2O_8^{2-} + Fe^{2+} \rightarrow SO_4^{\bullet-} + Fe^{3+} + SO_4^{2-} \quad (2)$$

Heterogeneous catalytic processes (HCPs), using iron-containing solids [hematite (iron(III) oxide, Fe_2O_3), magnetite (Fe_3O_4), etc.], have been considered to be efficient catalysts. HCPs have advantages, including low leaching of transition metals, lack of secondary pollution, and lack of sludge production. Hematite has been widely used as an efficient heterogeneous catalyst in the degradation of different pollutants. It is capable of activating persulfate and

improving its oxidation potential (Lin & Zhang 2017; Kermani *et al.* 2018).

Recent researchers have focused on combinative or hybrid techniques. The use of ultrasonic waves can enhance the performance of the hybrid system through persulfate activation and the formation of $H^{\bullet}$ and $OH^{\bullet}$ radicals (Ai *et al.* 2007; Lu *et al.* 2020). During ultrasonic irradiation, the development, growth and collapse of bubbles provide high pressures and temperatures in the aqueous solution that may directly degrade organic pollutants (Mosleh *et al.* 2018). Ultrasound irradiation can enhance the reaction mass transfer in solid-liquid interphases. In addition, ultrasonic irradiation reduces the consumption of chemicals such as oxidants and catalysts (Guo *et al.* 2017; Camargo-Perea *et al.* 2020). The hydroxyl radicals ($OH^{\bullet}$) and hydroperoxyl radicals ($HO_2^{\bullet}$) are generated during the cleavage of water molecules, as shown in Equations (3)–(8) (Mohapatra *et al.* 2010; Monteagudo *et al.* 2018):

$$H_2O +))) \rightarrow H^{\bullet} + OH^{\bullet} \quad (3)$$

$$H^{\bullet} + O_2 \rightarrow HO_2^{\bullet} \quad (4)$$

$$H^{\bullet} + H_2O \rightarrow OH^{\bullet} + H_2 \quad (5)$$

$$OH^{\bullet} + OH^{\bullet} \rightarrow H_2O_2 \quad (6)$$

$$H_2O_2 + OH^{\bullet} \rightarrow H_2O + HO_2^{\bullet} \quad (7)$$

$$H_2O_2 + H^{\bullet} \rightarrow H_2O + OH^{\bullet} \quad (8)$$

So far, studies have been carried out on the use of heterogeneous catalysts combined with UV and US irradiation as peroxymonosulfate and persulfate activators for the removal of different pollutants (Gobouri 2016; Liu *et al.* 2018; Tomić *et al.* 2019). Hematite nanoparticles (HNPs, α-Fe_2O_3), as heterogeneous activators, can effectively activate persulfate for the production of sulfate free radicals that are strong oxidants for the degradation of pollutants. No studies are available on the sonocatalytic degradation of emerging pollutants (EPs) such as BPA with activation of persulfate by HNPs. In the present study, the activation of persulfate was performed simultaneously by US irradiation and HNPs. The catalytic performance of the US/HNPs/PS system for the degradation of BPA was investigated under different operational parameters (pH, catalyst dose, PS dose, reaction time and pollutant concentration). After the optimization of the process, mineralization and reusability were also examined.

MATERIALS AND METHODS

Materials

BPA (purity $\geq$ 99%) was obtained from Sigma-Aldrich. Acetonitrile (CH_3CN, 99.9%), water (H_2O, 99.9%) and sodium persulfate ($Na_2S_2O_8$) were purchased from Merck. $FeCl_3.6H_2O$, urea, ammonium hydroxide, and ethanol (analytical reagent) were obtained from Merck and were used to prepare the hematite nanoparticles. For pH adjustment, sulfuric acid (H_2SO_4) and sodium hydroxide (NaOH) were used, which were provided from Sigma-Aldrich.

Synthesis of hematite nanoparticles

HNPs were synthesized by the hydrothermal method described by Ning *et al.* (2017). Briefly, 2.2 g $FeCl_3.6H_2O$ and 2 g urea were added to 50 mL distilled water. 25 mL of ammonium hydroxide, as the precipitating agent, was added dropwise with magnetic stirring. The solution was transferred into a Teflon-lined autoclave and then was heated at 150 °C for 12 hours. After cooling at room temperature, the resulting precipitation was washed with distilled water and ethanol several times. Finally, it was calcinated at 450 °C for 3 hours.

Characterization instruments

Scanning electron microscopy was performed to investigate the surface morphology of the nanoparticles using a field emission scanning electron microscopy (FESEM). To determine the crystalline structure of the synthesized nanoparticles, the XRD pattern was obtained using X-ray diffraction (XRD). The functional groups of hematite nanoparticles were determined by Fourier transform infrared spectroscopy (FTIR). Iron oxide nanoparticles were observed in electron micrographs obtained with transmission electron microscopy (TEM).

Experimental procedure

The experiments were done in 250 mL flask containing 100 mL of the sample with mechanical stirring at room temperature (25 ± 1 °C). The BPA stock solution (500 mg/L) was prepared by dissolving given amounts of BPA in deionized water. At each stage of the experiment, hematite nanoparticles were added to the BPA solution

and then a certain amount of sodium persulfate was added to the solution. The solution pH was adjusted by the addition of H_2SO_4 (0.1 M) or NaOH (0.1 M). The process was performed in different operational conditions including pH (3–11), BPA concentration (10–50 mg/L), persulfate concentration (1–5 mM), hematite nanoparticle dosage (0.005–0.02 g/L), ultrasonic power (100–300 W), and 30 min of reaction time.

The samples were collected during the reaction at different time intervals. A small volume of the solution (5 mL) was taken and each sample was filtered with 0.22-μm syringe filters. 0.5 mL methanol was added as the scavenger of $OH^{\bullet}$ and $SO_4^{\bullet-}$ for terminating the oxidation reaction.

After optimizing the process, to determine the dominant reactive species, quenching experiments were carried out in the presence of different scavenger compounds including methanol and *tert*-butyl alcohol. The mineralization of the US/HNPs/PS system based on chemical oxygen demand (COD) and the reusability of HNPs were also investigated. The kinetic models for BPA degradation by US/HNPs/PS system were examined.

Analytical methods

The pH measurements were done using a pH meter (Eutech 2700). The concentration of BPA was determined by high-performance liquid chromatography (HPLC) (KNAUER, Germany) with ultimate variable wavelength UV detector at 220 nm. The isocratic mobile phase consisted of acetonitrile and water with a ratio of 1:1 (50% Millipore water and 50% acetonitrile) at the flow rate of 1 mL/min^{-1} using a C18 column (Kromasil 100-5C18, 250 mm × 4.6 mm × 5 μm particle size). The retention time for BPA was 7.16–9.06 min. According to the calibration curve at different levels of BPA (0.1–50 mg/L), the R-squared was 0.9999. The limit of detection (LOD) and the limit of quantification (LOQ) were 0.01 mg/L and 0.1 mg/L, respectively.

The BPA removal efficiency (%) was calculated according to Equation (9):

$$R(\%) = \frac{(C_0 - C_t)}{C_0} \times 100 \tag{9}$$

where C_0 and C_t are initial and residual BPA concentrations (mg/L) at reaction time t (min) (Huang *et al.* 2014). COD was measured based on the standard methods for the examination of water and wastewater using a spectrophotometer (DR5000, HACH).

RESULTS AND DISCUSSION

Characterization of hematite nanoparticles

The FESEM image of HNPs is shown in Figure 1(a), and shows that the HNPs are spherical and have a diameter of less than 100 nm. The approximate crystallite size of nanoparticles (D) was calculated using Scherer's equation (Equation (10)):

$$D = \frac{0.9\lambda}{\beta \cos\theta} \tag{10}$$

where λ is the X-ray wavelength (1.540598 Å), β is the full width at half-maximum, and θ is the diffraction angle (Lassoued *et al.* 2017). The approximate crystallite size of HNPs was found to be in the range of 65.86–74.80 nm, which indicated that the surface of the hematite nanoparticles was almost porous and provided active sites for improving process efficiency.

The size and morphology of the HNPs were specified by TEM imaging (Figure 1(b). The image shows a particle size of 10–25 nm, which indicates that the HNPs easily aggregate to form larger particles or chain structures.

The results of the FTIR analysis of the nanoparticles are shown in Figure 1(c). The FTIR spectra indicate absorption peaks around 450–600 cm^{-1}, 1,400–1,600 cm^{-1} and 3,440 cm^{-1}. Two bands at 471 cm^{-1} and 585 cm^{-1} were ascribed to the Fe-O stretching mode of hematite. The absorption peaks at 1,405 cm^{-1}, 1,622 cm^{-1} and 3,440 cm^{-1} were related to the stretching and bending vibration of OH groups.

For characterizing the phase and crystallization, XRD measurement was done for the HNPs (Figure 1(d)). The XRD patterns show sharp peaks at 2θ values of 25, 33.51, 35.96, 41.26, 49.81, 54.36, 58.61, 62.76 and 64.31 that correspond to 012, 104, 110, 113, 024, 116, 018, 214, and 300. The crystalline structure of the HNPs was identified using the standard XRD pattern of hematite (JCPDS Card, no. 33-0664). No other crystalline phases of Fe_2O_3 or impurities were observed based on the XRD pattern, which indicates the pure HNP phase.

Comparison of alternative processes for BPA degradation

The degradation of BPA was performed by different processes under the same experimental conditions. As can be seen (Figure 2), the BPA degradation rate in single systems

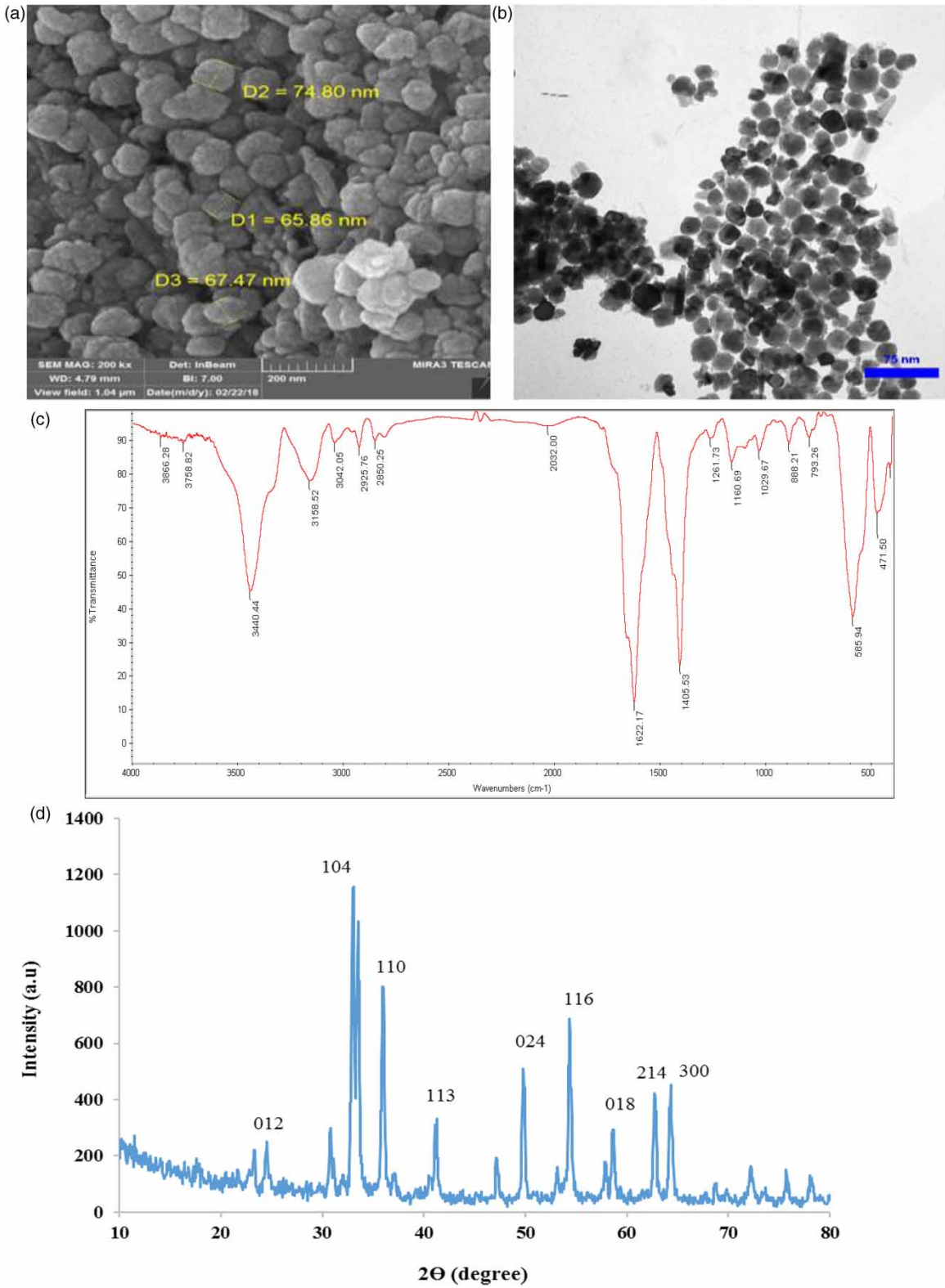

Figure 1 | Characterization of hematite nanoparticles. (a) FESEM image; (b) TEM image; (c) FTIR analysis; (d) XRD spectra.

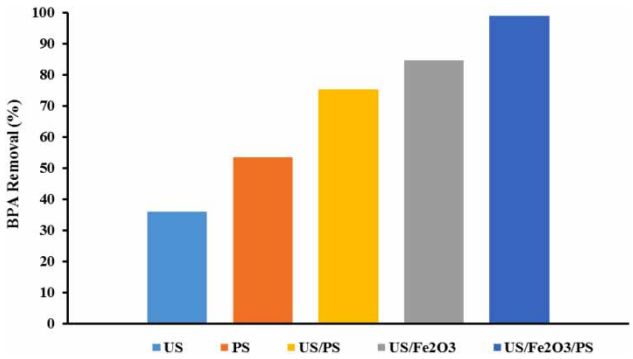

Figure 2 | The effect of different processes on BPA degradation (pH: 3, HNP dosage: 0.1 g/L, PS concentration: 1 mM, BPA concentration: 25 mg/L, US power: 200 W, reaction time: 60 min).

is lower than binary and ternary systems due to increasing the formation of the reactive radicals (˙OH and $SO_4^{\bullet-}$) in hybrid systems (Takdastan *et al.* 2018).

The results indicated that the removal efficiency of BPA was low under US irradiation alone (35.86%) and PS alone (53.54%). The removal efficiency using US/PS was 75.38%, whereas the US/HNPs and US/HNPs/PS systems could remove 84.60% and 98.87%, respectively.

Ultrasonic irradiation alone cannot provide a high degradation efficiency for organic contaminants. In the US/PS system, the heat induced by US can accelerate the decomposition of PS and facilitate the pollutant degradation (Lu *et al.* 2020). In the presence of Fe_2O_3 nanoparticles as a catalyst, ultrasonic irradiation provides a larger HNP surface area and the cavitation increases. Persulfate is relatively stable at room temperature, but adding nanoparticles leads to the activation of persulfate. The sulfate radical ($SO_4^{\bullet-}$) formed increases the process efficiency (Matzek & Carter 2016). The presence of a catalyst in the ultrasound system leads to an increase in the intensification of cavitational activity in the reactor and reduces the activation energy. The increase in the intensity of cavitation reduces the collapse pressure for a single cavity and increases the number of cavitation bubbles, thus improving the ultrasonic efficiency (Karim & Shriwastav 2020). When Fe_2O_3 is added to the system, fixed cavitation bubbles in the ultrasonic field explode asymmetrically on its surface, increasing the cavitation effect (Liu *et al.* 2020). When the catalyst and PS were used together, the degradation rate of BPA increased. This indicates that HNPs have a high capability of activating PS (Jiang *et al.* 2013). The combination of US and the HNPs/PS system improved the reaction effectiveness.

In addition to sulfate radicals, hydroxyl radicals (˙OH) are also formed, which result in increased efficiency (Jiang *et al.* 2013). OH˙ radicals are extremely active and have a strong oxidation potential. In the sonochemical reactor, the decomposition of the water molecule takes place by sonochemical waves and produces hydroxyl radicals. In the presence of US irradiation alone, a very small amount of ˙OH is formed, which leads to low removal efficiency (Wang *et al.* 2014). With the addition of the HNPs as a sonocatalyst, the degradation rate is increased as more water molecules are decomposed and more ˙OH produced as a result of the increase in the number of cavitation bubbles formed on the sonocatalyst surface (Khataee *et al.* 2018).

The effect of solution pH

The solution pH plays an important role in oxidation processes because of its effect on the surface properties and the ionization degree of the pollutant and oxidant (Kermani *et al.* 2018). The effect of pH (in the range of 3–11) on the degradation of BPA by the US/HNPs/PS process is shown in Figure 3. As can be seen, increasing pH in alkaline conditions led to reduction in degradation efficiency. For pH values of 3.0, 5.0, 7.0, 9.0 and 11.0, the degradation efficiencies at the reaction time of 30 min were 95.74%, 83.6%, 80.95%, 71.1% and 63.18%, respectively. The best decomposition was obtained in acidic conditions (pH: 3.0).

At higher pH values, because of the catalyst deactivation caused by the formation of ferric hydroxide complexes, PS molecules were less activated by the catalyst and BPA degradation was decreased. Similar results have been presented in the other studies for the degradation of various pollutants (Ghauch *et al.* 2012; Kermani *et al.* 2018).

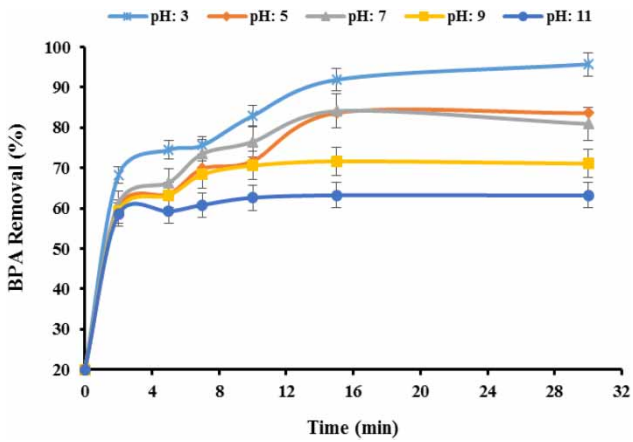

Figure 3 | The effect of pH on BPA removal (HNP dosage: 0.01 g/L, PS concentration: 3 mM, BPA concentration: 25 mg/L, US power: 200 W).

In acidic conditions (pH < 7), sulfate radicals are dominant. They have a higher oxidation potential than hydroxyl radicals, therefore the removal efficiency is higher in acidic pH (Equations (11)–(13)) (Matzek & Carter 2016).

$$S_2O_8^{2-} + H^+ \rightarrow HS_2O_8^- \quad (11)$$

$$\text{Acidic conditions: } HS_2O_8^- \rightarrow SO_4^{2-} + SO_4^{-\bullet} + H^+ \quad (12)$$

$$\text{Alkaline conditions: } SO_4^{-\bullet} + OH^- \rightarrow H^+ + SO_4^{2-} + OH^\bullet \quad (13)$$

The pKa value of BPA (9.6 and 10.2) can be a reason for the increase in degradation efficiency under acidic conditions. At pH = 3.0, BPA exists in its cationic state and becomes positive, which leads to a strong electrostatic repulsion between the positively charged BPA molecules and the negatively charged catalyst (Gültekin & Ince 2008; Gobouri 2016). Therefore, pH = 3.0 was considered to be the optimal pH for the next steps of the experiments.

The effect of sodium persulfate concentration

The effect of different concentrations of PS (1–5 mM) on BPA degradation by US/HNPs was investigated. With increasing PS concentration (from 1 to 4 mM) at 15 min intervals, the removal efficiency was increased from 75.21% to 96.2% (Figure 4(a)). At higher PS dosages, more sulfate radicals were formed, resulting in higher degradation rates. These results are consistent with results from other studies (Monteagudo *et al.* 2018; Takdastan *et al.* 2018). However, the degradation rate was 75.8% at PS 5 mM. This was because of (a) the recombination of $SO_4^{\bullet-}$ and $OH^\bullet$ radicals (Equations (14) and (15)); (b) the reaction between excess persulfate and $SO_4^{\bullet-}$ (Equation (16));

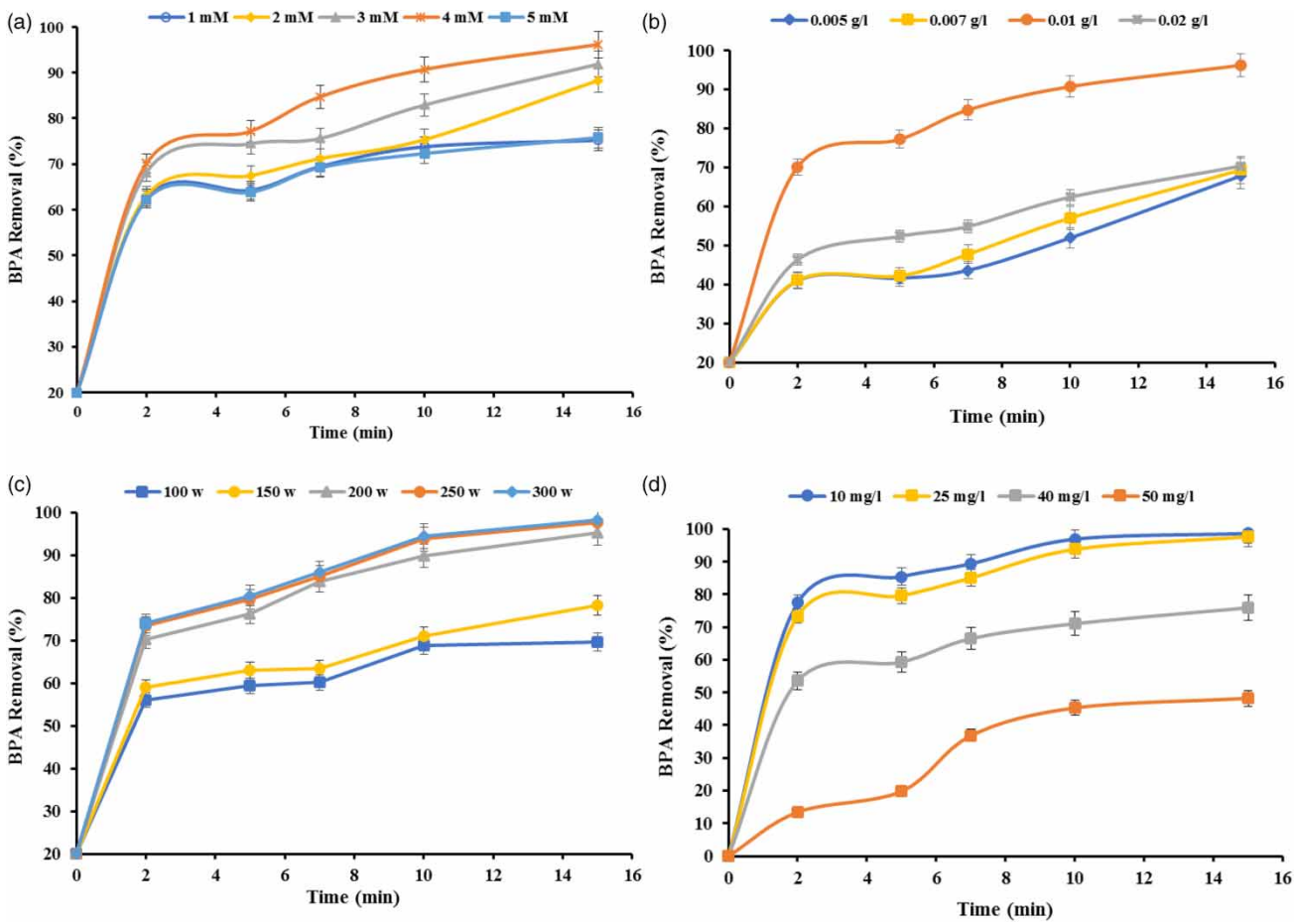

Figure 4 | The effect of (a) PS concentration on BPA removal (pH: 3, initial BPA concentration: 25 mg/L, catalyst dosage: 0.01 g/L, US power: 200 W), (b) catalyst dosage on BPA removal (pH: 3, PS concentration: 4 Mm, BPA concentration: 25 mg/L, US power: 200 W), (c) US power on BPA removal (pH: 3, PS concentration: 4 Mm, BPA concentration: 25 mg/L, catalyst dosage: 0.01 g/L), (d) BPA initial concentration on BPA removal (pH: 3, PS concentration: 4 Mm, catalyst dosage: 0.01 g/L, US power: 250 W).

and (c) unproductive persulfate activation (Equation (17)) (Kermani *et al.* 2018; Monteagudo *et al.* 2018).

$$SO_4^{\bullet-} + SO_4^{\bullet-} \rightarrow S_2O_8^{2-} \quad (14)$$

$$OH^{\bullet} + OH^{\bullet} \rightarrow H_2O_2 \quad (15)$$

$$SO_4^{\bullet-} + S_2O_8^{2-} \rightarrow SO_4^{2-} + S_2O_8^{\bullet-} \quad (16)$$

$$S_2O_8^{2-} + OH^{\bullet} \rightarrow S_2O_8^{\bullet-} + OH^{-} \quad (17)$$

The effect of catalyst dosage

The optimization of the catalyst dosage is important because of forming a dispersed suspension in combination with organic pollutants. Different dosages of HNPs (0.005–0.02 g/L) were investigated for the removal efficiency of BPA. As can be seen (Figure 4(b)), for dosages of 0.005, 0.007, 0.01 and 0.02 g/L at the reaction time of 15 min, the degradation rates were 67.84%, 69.37%, 96.02% and 70.36%, respectively.

According to the results, by the addition of various dosages of HNPs up to 0.01 g/L, the degradation rate of BPA increased, which can be attributed to an increase in the production of hydroxyl and sulfate radicals. At higher dosages, more active sites are provided that lead to the higher rates of PS activation and generation of sulfate radicals (Kermani *et al.* 2018). The maximum efficiency (96.2%) was achieved with the catalyst dosage 0.01 g/L.

At doses higher than 0.01 g/L, the degradation rate was decreased. This is attributed to lower exploitation of active sites on the catalyst surface. At higher catalyst dosages, the production of aggregates and subsequent self-binding of catalyst particles lead to the reduction of active sites (Kermani *et al.* 2018; Takdastan *et al.* 2018).

The effect of ultrasonic power

Figure 4(c) shows the effect of various levels of ultrasonic power on the degradation rate of BPA. As observed, BPA removal increased by increasing the ultrasonic power from 100 W (69.55%) to 300 W (98.02%). During the US irradiation, the tiny gas bubbles in water can form, grow and collapse (Hu & Long 2016). At higher ultrasonic power, the pulsation and collapse of bubbles increased, causing a higher generation of the cavitation bubbles and reactive radicals. At higher ultrasonic power, more turbulence improved the mass transfer in the solution (Gao *et al.* 2018; Monteagudo *et al.* 2018).

At the ultrasonic power levels higher than 250 W a very slight increase in BPA degradation efficiency was observed. Above an optimal or critical ultrasonic power amount, a cloud of the cavitation bubbles forms but hardly collapses. In addition, it disperses the formation of sound waves that lead to a little increase in removal efficiency (Camargo-Perea *et al.* 2020).

There was no significant difference between the removal efficiencies for the ultrasonic power of 250 W (97.64%) and 300 W (98.02%), so 250 W was selected as the optimum level.

Effect of the BPA initial concentration

The effect of various BPA concentrations on the removal efficiency was studied (Figure 4(d)). It can be seen that the removal efficiency decreased at concentrations higher than 10 mg/L. So for the initial concentration of 50 mg/L at a reaction time of 15 min, the removal efficiency was 48.27%. The maximum removal efficiency (98.64%) was obtained for the BPA concentration of 10 mg/L. The production of less hydroxyl radicals at higher concentrations and subsequently, the decreasing reactions between BPA and $OH^{\bullet}$ radicals results in a decrease of the degradation rate. In addition, at high concentrations, there may occur a competitive reaction for $OH^{\bullet}$ and $SO_4^{\bullet-}$ radicals between BPA and the intermediates (Li *et al.* 2021).

Kinetics for sonocatalytic activity of HNPs

In order to determine the reaction rate, the pseudo-first-order kinetic model was studied. Based on the results (Figure 5), under the optimal conditions, the BPA degradation was fitted by Equation (18).

$$-\mathrm{Ln}\frac{C}{C_0} = k_{obs}t \quad (18)$$

where C_0 and C are the initial concentration and concentration of BPA at time t, t is the reaction time (min) and k_{obs} (the slope of obtained from the plot of $\mathrm{Ln}C/C_0$ versus elapsed time) is the rate constant (min^{-1}) (Li *et al.* 2016). The results showed that by increasing the initial concentration of, the pseudo-first-order kinetic rate of BPA degradation decreased. This may have been due to the production of less reactive species at the higher concentrations. The constant values of the pseudo-first-order

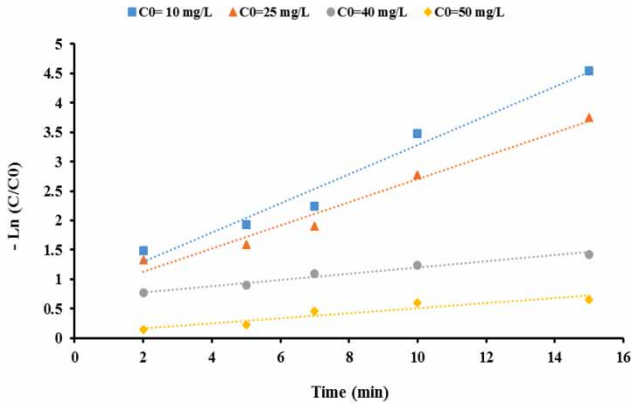

Figure 5 | The plot of Ln(C/C_0) against t for the different initial concentrations of BPA (pH: 3, PS concentration: 4 Mm, catalyst dosage: 0.01 g/L, US power: 250 W).

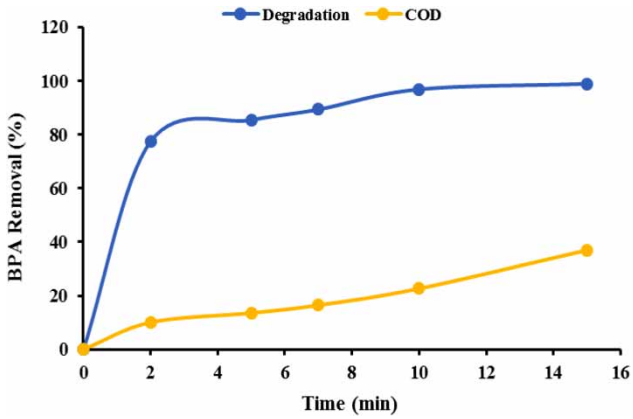

Figure 6 | The BPA mineralization (pH: 3, PS concentration: 4 mM, catalyst dosage: 0.01 g/L, initial BPA concentration: 10 mg/L, US power: 250 W).

kinetic model of BPA are presented in Table 1. By increasing the initial concentration of BPA from 10 to 50 mg/L, the k_{obs} rate was decreased from 0.2485 to 0.043.

Mineralization

The BPA mineralization (based on COD reduction) in the US/HNPs/PS process was determined under optimized conditions (pH: 3.0, PS concentration: 4 Mm, initial BPA concentration: 10 mg/L, catalyst dosage: 0.01 g/L, US power: 250 W). According to the results (Figure 6), the mineralization degree was 36.98% after 15 min. The organic chemical reaction with radicals leads to partial mineralization. In the study by Kermani *et al.* (2018), the mineralization degree was 36% for the degradation of both 2,4-D and MCPA herbicides using HNPs/PS. They stated that low efficiency can be due to the difficulty of completely removing the by-products formed, which requires more oxidation (Kermani *et al.* 2018).

Table 1 | The constant values of the pseudo-first-order kinetic model of BPA

Initial concentration of BPA (mg/L)	Constant (min^{-1})	Value
10	k_{obs}	0.2485
	R^2	0.9724
25	k_{obs}	0.1967
	R^2	0.9723
40	k_{obs}	0.0521
	R^2	0.9739
50	k_{obs}	0.043
	R^2	0.879

Reusability of the catalyst

The reusability of the catalyst is one of the key factors for the development and application of a catalyst at industrial scale. In order to evaluate the possibility of catalyst reuse, experiments were done for three consecutive cycles under the same conditions. For this purpose, HNPs were separated by a centrifuge and then washed with double distilled water several times and dried after each run. The obtained results are presented in Figure 7. The removal efficiency decreased after three cycles. The findings showed the removal efficiency of 98.64% at the first run. The removal value reached to 86.34% after the third run. This slight decrease could be because of a reduction in the catalyst adsorption capacity and HNP mass loss on the surface of the catalyst (Xu *et al.* 2016). Thus, HNPs have good reusability for several runs.

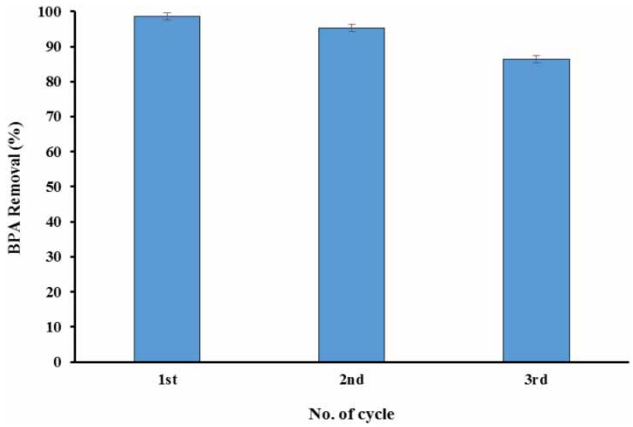

Figure 7 | The reusability of HNPs for BPA removal (pH: 3, PS concentration: 4 mM, catalyst dosage: 0.01 g/L, US power: 250 W).

Effect of scavengers

To identify the dominating radical species, quenching experiments were done using two organic compounds. Methanol (MeOH) and *tert*-butyl alcohol (TBA) have been extensively employed previously as scavengers of $SO_4^{\bullet-}$ and $OH^{\bullet}$ radicals due to their different reactivity with radicals (MeOH: $k_{SO4^{\bullet-}+MeOH} = 3.2 \times 10^6\ M^{-1}s^{-1}$ and $k_{OH^{\bullet}+MeOH} = 9.7 \times 10^8\ M^{-1}s^{-1}$, TBA: $k_{SO4^{\bullet-}+TBA} = 4 \times 10^5\ M^{-1}s^{-1}$ and $k_{OH^{\bullet}+TBA} = 7.6 \times 10^8\ M^{-1}s^{-1}$) (Buxton *et al.* 1988; Huang *et al.* 2014; Gu *et al.* 2015; Oh *et al.* 2016).

In the absence of the scavengers, 98.64% of BPA was removed. According to the results (Figure 8), in the presence of methanol, the degradation rate was reduced to 69.15%. The decrease in removal efficiency in the presence of methanol as a hydroxyl and sulfate radical scavenger confirmed that sulfate radicals might be the active species. In the case of TBA addition, the removal rate was 63.65%. TBA has a good reactivity with hydroxyl radicals and is a specific scavenger for $OH^{\bullet}$. The decreasing BPA degradation in the presence of TBA indicates that the $OH^{\bullet}$ may be one of the radicals involved (Gu *et al.* 2015; Oh *et al.* 2016). The results indicated that both $SO_4^{\bullet-}$ and $OH^{\bullet}$ radicals were responsible for BPA degradation using the US/HNPs/PS process.

Effect of anions

The presence of anions in natural aquatic environments affects the catalytic performance of AOPs. Therefore, the effect of anions such as chloride (Cl^-), sulfate (SO_4^{2-}) and hydrogen phosphate (HPO_4^{2-}) were evaluated on the degradation of BPA by the US/HNPs/PS system (Figure 9). In the absence of anions, the removal efficiency was 98.64%. The removal efficiencies were reduced to 83.58%, 61.6% and 51.81% in the presence of Cl^-, SO_4^{2-} and HPO_4^{2-}, respectively. The inhibition of the anions was in order of $Cl^- < SO_4^{2-} < HPO_4^{2-}$. The anions act as a scavengers of free radicals and form weaker radical species, which is how they reduce the removal efficiency of the pollutant (Golshan *et al.* 2018).

The reason for the slight inhibitory effect of the chloride ion is the reaction between the sulfate radical and the chloride ion that leads to the production of the chlorine radical. The generation of active chlorine species during the reactions of free radicals with the chloride ion are based on Equations (19)–(22). The chlorine radicals ($Cl^{\bullet}$, $Cl_2^{\bullet-}$) have lower redox potentials in comparison to sulfate and hydroxyl radicals (Golshan *et al.* 2018).

$$SO_4^{\bullet-} + Cl^- \rightarrow Cl^{\bullet} + SO_4^{2-} \quad (19)$$

$$Cl^{\bullet} + Cl^- \rightarrow Cl_2^{\bullet-} \quad (20)$$

$$Cl_2^{\bullet-} + Cl_2^{\bullet-} \rightarrow 2Cl^- + Cl_2 \quad (21)$$

$$Cl^{\bullet} + Cl^{\bullet} \rightarrow Cl_2 \quad (22)$$

The low inhibiting effect of the sulfate ion (SO_4^{2-}) can be attributed to the scavenging of hydroxyl radicals by the sulfate ions and the formation of the inevitable product of sulfate radicals in this system (Equation (23)) (Gao *et al.* 2018; Golshan *et al.* 2018).

$$SO_4^{2-} + OH^{\bullet} \rightarrow SO_4^{\bullet-} + OH^- \quad (23)$$

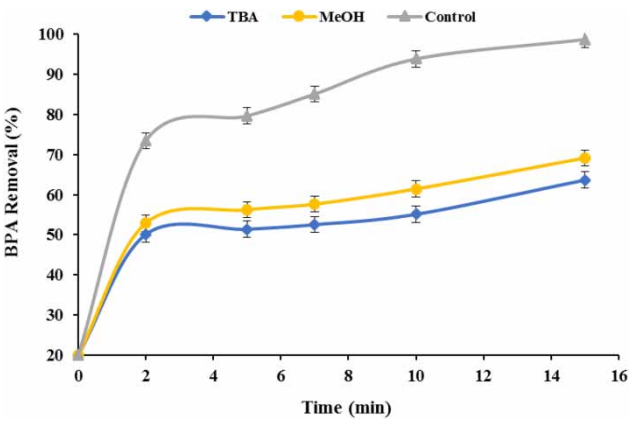

Figure 8 | The effect of radical scavengers on BPA removal (pH: 3, PS concentration: 4 Mm, catalyst dosage: 0.01 g/L, US power: 250 W, scavengers: 1 M).

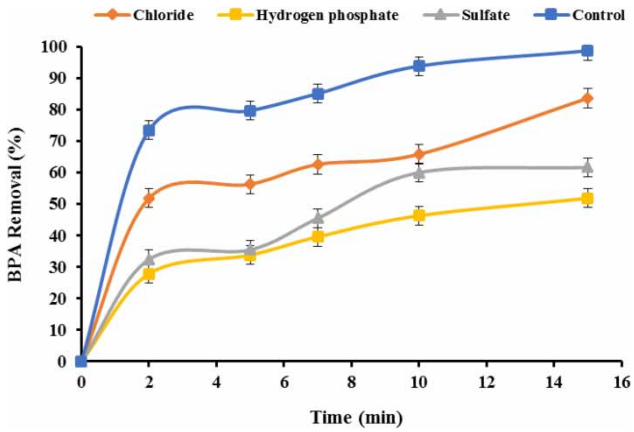

Figure 9 | The effect of anions on BPA removal (pH: 3, PS concentration: 4 mM, catalyst dosage: 0.01 g/L, US power: 250 W, anions: 3 mM).

Hydrogen phosphate (HPO_4^{2-}) has a greater inhibitory effect than sulfate and chloride ions due to the production of the hydrogen phosphate radical by electron transfer (Equation (24)). Also, these ions act as sulfate radical scavengers and reduce active sites on the catalyst by blocking the pores (Gao *et al.* 2018; Takdastan *et al.* 2018). The significant inhibitory impact of HPO_4^{2-} also can be attributed to the strong capability of phosphate to act as a complexing agent for iron or occupy a catalyst's active sites in heterogeneous systems (Li *et al.* 2021).

$$SO_4^{\bullet-} + HPO_4^{2-} \rightarrow H_2PO_4^{\bullet} + SO_4^{2-} \quad (24)$$

CONCLUSION

In this study, the catalytic application of HNPs for persulfate activation in the presence of US was investigated. US irradiation improved the performance of HNPs/PS in BPA degradation. The maximum removal efficiency was achieved at pH 3, PS concentration of 4 mM, catalyst dosage of 0.01 g/L and US power of 250 W at 15 min. Further increase in the ultrasonic power from the optimal amount leads to slight changes in degradation efficiency. In general, in terms of the ultrasonic power, typically optimum levels of ultrasonic power are recommended. The quenching tests indicated that both $OH^{\bullet}$ and $SO_4^{\bullet-}$ radicals may be the oxidizing species involved in the BPA degradation in the US/HNPs/PS process. The catalyst showed good reusability after three cycles. The mineralization rate under optimum experimental conditions was 36.98%. Results showed an inhibition in the degradation of BPA for all studied anions. Chloride and sulfate played a minor role in the decrease of efficiency in comparison with hydrogen phosphate. The kinetics of the catalytic oxidation of BPA by US/HNPs/PS was in good agreement with the pseudo-first-order model. Hematite nanoparticles (α-Fe_2O_3) are reusable and efficient nanoparticles for the catalytic degradation of BPA.

ACKNOWLEDGEMENTS

This research project has been financially supported by the Environmental Technologies Research Center, Ahvaz Jundishapur University of Medical Sciences (Grant no. ETRC 9626).

DATA AVAILABILITY STATEMENT

All relevant data are included in the paper or its Supplementary Information.

REFERENCES

Ai, Z., Lu, L., Li, J., Zhang, L., Qiu, J. & Wu, M. 2007 Fe@ Fe_2O_3 core–shell nanowires as iron reagent. 1. efficient degradation of rhodamine B by a novel sono-fenton process. *The Journal of Physical Chemistry C* **111** (11), 4087–4093.

Buxton, G. V., Greenstock, C. L., Helman, W. P. & Ross, A. B. 1988 Critical review of rate constants for reactions of hydrated electrons, hydrogen atoms and hydroxyl radicals (·OH/·O− in aqueous solution. *Journal of Physical and Chemical Reference Data* **17** (2), 513–886.

Camargo-Perea, A. L., Rubio-Clemente, A. & Peñuela, G. A. 2020 Use of ultrasound as an advanced oxidation process for the degradation of emerging pollutants in water. *Water* **12** (4), 1068.

Escalona, I., Fortuny, A., Stueber, F., Bengoa, C., Fabregat, A. & Font, J. 2014 Fenton coupled with nanofiltration for elimination of bisphenol A. *Desalination* **345**, 77–84.

Gao, Y.-q., Gao, N.-y., Wang, W., Kang, S.-f., Xu, J.-h., Xiang, H.-m. & Yin, D.-q. 2018 Ultrasound-assisted heterogeneous activation of persulfate by nano zero-valent iron (nZVI) for the propranolol degradation in water. *Ultrasonics Sonochemistry* **49**, 33–40.

Ghauch, A., Tuqan, A. M., Kibbi, N. & Geryes, S. 2012 Methylene blue discoloration by heated persulfate in aqueous solution. *Chemical Engineering Journal* **213**, 259–271.

Gobouri, A. A. 2016 Ultrasound enhanced photocatalytic properties of α-Fe_2O_3 nanoparticles for degradation of dyes used by textile industry. *Research on Chemical Intermediates* **42** (5), 5099–5113.

Golshan, M., Kakavandi, B., Ahmadi, M. & Azizi, M. 2018 Photocatalytic activation of peroxymonosulfate by TiO_2 anchored on cupper ferrite (TiO_2@$CuFe_2O_4$) into 2, 4-D degradation: process feasibility, mechanism and pathway. *Journal of Hazardous Materials* **359**, 325–337.

Gu, X., Lu, S., Guo, X., Sima, J., Qiu, Z. & Sui, Q. 2015 Oxidation and reduction performance of 1,1,1-trichloroethane in aqueous solution by means of a combination of persulfate and zero-valent iron. *RSC Advances* **5** (75), 60849–60856.

Guan, Y.-H., Ma, J., Ren, Y.-M., Liu, Y.-L., Xiao, J.-Y., Lin, L.-q. & Zhang, C. 2013 Efficient degradation of atrazine by magnetic porous copper ferrite catalyzed peroxymonosulfate oxidation via the formation of hydroxyl and sulfate radicals. *Water Research* **47** (14), 5431–5438.

Gültekin, I. & Ince, N. H. 2008 Ultrasonic destruction of bisphenol-A: the operating parameters. *Ultrasonics Sonochemistry* **15** (4), 524–529.

Guo, J., Zhu, L., Sun, N. & Lan, Y. 2017 Degradation of nitrobenzene by sodium persulfate activated with zero-valent

zinc in the presence of low frequency ultrasound. *Journal of the Taiwan Institute of Chemical Engineers* **78**, 137–143.

Hu, P. & Long, M. 2016 Cobalt-catalyzed sulfate radical-based advanced oxidation: a review on heterogeneous catalysts and applications. *Applied Catalysis B: Environmental* **181**, 103–117.

Huang, Y., Wong, C., Zheng, J., Bouwman, H., Barra, R., Wahlström, B., Neretin, L. & Wong, M. 2012 Bisphenol A (BPA) in China: a review of sources, environmental levels, and potential human health impacts. *Environment International* **42**, 91–99.

Huang, R., Fang, Z., Fang, X. & Tsang, E. P. 2014 Ultrasonic Fenton-like catalytic degradation of bisphenol A by ferroferric oxide (Fe_3O_4) nanoparticles prepared from steel pickling waste liquor. *Journal of Colloid and Interface Science* **436**, 258–266.

Huang, D., Zhang, G., Yi, J., Cheng, M., Lai, C., Xu, P., Zhang, C., Liu, Y., Zhou, C., Xue, W., Wang, R., Li, Z. & Chen, S. 2021 Progress and challenges of metal-organic frameworks-based materials for SR-AOPs applications in water treatment. *Chemosphere* **263**, 127672.

Ji, F., Li, C. & Deng, L. 2011 Performance of CuO/Oxone system: heterogeneous catalytic oxidation of phenol at ambient conditions. *Chemical Engineering Journal* **178**, 239–243.

Jiang, X., Wu, Y., Wang, P., Li, H. & Dong, W. 2013 Degradation of bisphenol A in aqueous solution by persulfate activated with ferrous ion. *Environmental Science and Pollution Research* **20** (7), 4947–4953.

Karim, A. V. & Shriwastav, A. 2020 Degradation of ciprofloxacin using photo, sono, and sonophotocatalytic oxidation with visible light and low-frequency ultrasound: degradation kinetics and pathways. *Chemical Engineering Journal* **392**, 124853.

Kermani, M., Mohammadi, F., Kakavandi, B., Esrafili, A. & Rostamifasih, Z. 2018 Simultaneous catalytic degradation of 2,4-D and MCPA herbicides using sulfate radical-based heterogeneous oxidation over persulfate activated by natural hematite (α-Fe_2O_3/PS). *Journal of Physics and Chemistry of Solids* **117**, 49–59.

Khataee, A., Gholami, P., Kalderis, D., Pachatouridou, E. & Konsolakis, M. 2018 Preparation of novel CeO_2-biochar nanocomposite for sonocatalytic degradation of a textile dye. *Ultrasonics Sonochemistry* **41**, 503–513.

Kusic, H., Peternel, I., Ukic, S., Koprivanac, N., Bolanca, T., Papic, S. & Bozic, A. L. 2011 Modeling of iron activated persulfate oxidation treating reactive azo dye in water matrix. *Chemical Engineering Journal* **172** (1), 109–121.

Lassoued, A., Dkhil, B., Gadri, A. & Ammar, S. 2017 Control of the shape and size of iron oxide (α-Fe_2O_3) nanoparticles synthesized through the chemical precipitation method. *Results in Physics* **7**, 3007–3015.

Li, T., Abdelhaleem, A., Chu, W. & Xu, W. 2021 Efficient activation of oxone by pyrite for the degradation of propanil: kinetics and degradation pathway. *Journal of Hazardous Materials* **403**, 1–11.

Li, X., Wang, Z., Zhang, B., Rykov, A. I., Ahmed, M. A. & Wang, J. 2016 $Fe_xCo_{3-x}O_4$ nanocages derived from nanoscale metal–organic frameworks for removal of bisphenol A by activation of peroxymonosulfate. *Applied Catalysis B: Environmental* **181**, 788–799.

Lin, K.-Y. A. & Zhang, Z.-Y. 2017 Degradation of bisphenol A using peroxymonosulfate activated by one-step prepared sulfur-doped carbon nitride as a metal-free heterogeneous catalyst. *Chemical Engineering Journal* **313**, 1320–1327.

Liu, J., Zhao, Z., Shao, P. & Cui, F. 2015 Activation of peroxymonosulfate with magnetic Fe_3O_4–MnO_2 core–shell nanocomposites for 4-chlorophenol degradation. *Chemical Engineering Journal* **262**, 854–861.

Liu, Y., Sun, N., Hu, J., Li, S. & Qin, G. 2018 Photocatalytic degradation properties of α-Fe_2O_3 nanoparticles for dibutyl phthalate in aqueous solution system. *Royal Society Open Science* **5** (4), 172196.

Liu, L., Yang, C., Tan, W. & Wang, Y. 2020 Degradation of acid Red 73 by activated persulfate in a heat/Fe_3O_4@AC system with ultrasound intensification. *ACS Omega* **5** (23), 13739–13750.

Lu, X., Qiu, W., Peng, J., Xu, H., Wang, D., Cao, Y., Zhang, W. & Ma, J. 2020 A review on additives-assisted ultrasound for organic pollutants degradation. *Journal of Hazardous Materials* **403**, 1–12.

Matzek, L. W. & Carter, K. E. 2016 Activated persulfate for organic chemical degradation: a review. *Chemosphere* **151**, 178–188.

Mohapatra, D., Brar, S., Tyagi, R. & Surampalli, R. 2010 Physico-chemical pre-treatment and biotransformation of wastewater and wastewater sludge–fate of bisphenol A. *Chemosphere* **78** (8), 923–941.

Mokhtari, S. A., Farzadkia, M., Esrafili, A., Kalantari, R. R., Jafari, A. J., Kermani, M. & Gholami, M. 2016 Bisphenol A removal from aqueous solutions using novel UV/persulfate/H_2O_2/Cu system: optimization and modelling with central composite design and response surface methodology. *Journal of Environmental Health Science and Engineering* **14** (1), 19.

Monteagudo, J., El-taliawy, H., Durán, A., Caro, G. & Bester, K. 2018 Sono-activated persulfate oxidation of diclofenac: degradation, kinetics, pathway and contribution of the different radicals involved. *Journal of Hazardous Materials* **357**, 457–465.

Mosleh, S., Rahimi, M. R., Ghaedi, M., Dashtian, K. & Hajati, S. 2018 Sonochemical-assisted synthesis of CuO/Cu_2O/Cu nanoparticles as efficient photocatalyst for simultaneous degradation of pollutant dyes in rotating packed bed reactor: LED illumination and central composite design optimization. *Ultrasonics Sonochemistry* **40**, 601–610.

Ning, P., Song, X., Li, K., Wang, C., Tang, L. & Sun, X. 2017 Catalytic hydrolysis of carbonyl sulphide and carbon disulphide over Fe_2O_3 cluster: competitive adsorption and reaction mechanism. *Scientific Reports* **7** (1), 14452.

Oh, W.-D., Dong, Z. & Lim, T.-T. 2016 Generation of sulfate radical through heterogeneous catalysis for organic contaminants removal: current development, challenges and prospects. *Applied Catalysis B: Environmental* **194**, 169–201.

Rochester, J. R. 2013 Bisphenol A and human health: a review of the literature. *Reproductive Toxicology* **42**, 132–155.

Staples, C. A., Dome, P. B., Klecka, G. M., Oblock, S. T. & Harris, L. R. 1998 A review of the environmental fate, effects, and exposures of bisphenol A. *Chemosphere* **36** (10), 2149–2173.

Takdastan, A., Kakavandi, B., Azizi, M. & Golshan, M. 2018 Efficient activation of peroxymonosulfate by using ferroferric oxide supported on carbon/UV/US system: a new approach into catalytic degradation of bisphenol A. *Chemical Engineering Journal* **331**, 729–743.

Tomić, N. Z., Vuksanović, M. M., Veljović, Đ., Đokić, V., Marinković, A. D. & Heinemann, R. J. 2019 Photocatalytic degradation of bisphenol a with α-Fe_2O_3 fibers and particles. *Science of Sintering* **51** (3), 265–276.

Vandenberg, L. N., Maffini, M. V., Sonnenschein, C., Rubin, B. S. & Soto, A. M. 2009 Bisphenol-A and the great divide: a review of controversies in the field of endocrine disruption. *Endocrine Reviews* **30** (1), 75–95.

Wang, X., Wang, L., Li, J., Qiu, J., Cai, C. & Zhang, H. 2014 Degradation of Acid Orange 7 by persulfate activated with zero valent iron in the presence of ultrasonic irradiation. *Separation and Purification Technology* **122**, 41–46.

Xu, Y., Ai, J. & Zhang, H. 2016 The mechanism of degradation of bisphenol A using the magnetically separable $CuFe_2O_4$/peroxymonosulfate heterogeneous oxidation process. *Journal of Hazardous Materials* **309**, 87–96.

First received 14 August 2020; accepted in revised form 28 November 2020. Available online 14 December 2020